Dynamics of a Ground-State Cooled Ion Colliding with Ultracold Atoms

Ziv Meir,[†] Tomas Sikorsky, Ruti Ben-shlomi, Nitzan Akerman, Yehonatan Dallal, and Roee Ozeri
Department of Physics of Complex Systems, Weizmann Institute of Science, Rehovot 7610001, Israel
(Received 10 July 2016; published 7 December 2016)

Ultracold atom-ion mixtures are gaining increasing interest due to their potential applications in ultracold and state-controlled chemistry, quantum computing, and many-body physics. Here, we studied the dynamics of a single ground-state cooled ion during few, to many, Langevin (spiraling) collisions with ultracold atoms. We measured the ion's energy distribution and observed a clear deviation from the Maxwell-Boltzmann distribution, characterized by an exponential tail, to a power-law distribution best described by a Tsallis function. Unlike previous experiments, the energy scale of atom-ion interactions is not determined by either the atomic cloud temperature or the ion's trap residual excess-micromotion energy. Instead, it is determined by the force the atom exerts on the ion during a collision which is then amplified by the trap dynamics. This effect is intrinsic to ion Paul traps and sets the lower bound of atom-ion steady-state interaction energy in these systems. Despite the fact that our system is eventually driven out of the ultracold regime, we are capable of studying quantum effects by limiting the interaction to the first collision when the ion is initialized in the ground state of the trap.

DOI: 10.1103/PhysRevLett.117.243401

Since its first inception [1–3], observing quantum mechanical phenomena was one of the important goals of hybrid atom-ion research [4–10]. The polarization potential between atoms and ions scales as r^{-4} and extends to hundreds of nm. Similarly to other forms of atomic interaction, it exhibits quantum features such as Feshbach [11,12] and shape resonances [13] at sufficiently low temperatures; however, due to its long length scale, it is also predicted to form macroscopic objects [14]. Ultracold atom-ion systems are an appealing new platform for performing quantum computation [15,16] and many-body physics [17]. However, all experiments so far have relied on sympathetic cooling of the ion by the atomic cloud and were limited to the mK energy scale [18] and above.

The interplay between the ion's radio-frequency (rf) trap oscillating electric fields and sympathetic cooling has been known for a long time [19]. However, only recently the full understanding of this dynamical system is beginning to be revealed [20]. In particular, it was theoretically shown that sympathetic cooling of the ion results in a nonthermal energy distribution with a power-law tail, the magnitude of which depends on the atom-ion mass ratio and trap parameters [21–25]. This phenomenon is closely related, among other examples, to anomalous diffusion in optical lattices [26] and is well described by non-Maxwellian statistics, which was introduced by Tsallis [27]. If the ion is sufficiently lighter than the cooling atoms, its mean energy diverges and collisions eventually result in ion loss from the trap.

In stable mixtures the mean steady-state energy of the ion is proportional, albeit with potentially a large amplification factor, to the energy of a single collision at the trap center, which is determined by, e.g., residual excess micromotion (EMM) [22] or the atoms' temperature [23]. It is therefore interesting to ask what would determine the steady-state temperature and ion dynamics when the ion is initialized in the ground state of the trap and both the ion's EMM and the atoms' temperature are negligible? Recently, the energy involved in a single collision was calculated to be determined by the atom-ion attraction during collision, which pulls the ion away from the trap minimum into finite rf regions of the trap [28]. Furthermore, the quantum dynamics of ultracold atom-ion collisions was calculated and has shown significant heating that depends on the trap parameters used [29].

In this experiment, we studied the dynamics of an ion, initialized in the ground state of all trap modes, during collisions with ultra-cold atoms and negligible EMM, thus investigating the fundamental limits to the temperature of atom-ion mixtures in Paul traps. The species we used are ^{87}Rb atoms and $^{88}Sr^{+}$ ion, which have almost equal masses, in contrast to previous experiments where light atoms and heavy ions were used. This choice of masses amplifies the deviation from Maxwell-Boltzmann to a power-law energy distribution, which was not observed in experiments before. Our results show a clear deviation from Maxwell-Boltzmann to a power-law distribution best described by a Tsallis function. Moreover, the heating observed is consistent with that generated by the pulling of the ion from the trap center calculated by molecular dynamics simulations.

During a collision the atom is polarized by the electric field of the ion, leading to an attractive potential $V(r) = -C_4/2r^4$. Here, r is the atom-ion separation and C_4 determines the interaction strength. Classically, collisions can be divided into glancing collisions, which are purely elastic and involve only small momentum transfer and Langevin (spiraling) collisions which transfer large momentum and can also lead to inelastic processes such as spin exchange or relaxation [30], charge exchange [31],

 © 2016 American Physical Society

molecule formation [7], and three-body recombination [32]. While the loss of atoms from the trap in the presence of an ion is dominated by glancing collisions [22], we expect the heating of the ion to be dominated by the large momentum transfer of Langevin collisions, the rate of which is energy independent for the r^{-4} potential. For our experimental parameters the mean time between Langevin collisions is 0.35 ms. The rate of charge exchange and three-body collisions is suppressed by 4–5 orders of magnitude compared with that of elastic Langevin collisions, such that they do not play a significant role.

During collisions the ion's energy distribution develops a power-law tail [21–23,33]. We use the Tsallis distribution [27], which is a generalization of the thermal Maxwell-Boltzmann distribution, to fit both our simulation [34] and experiment results:

$$P(E) = \frac{(n-3)(n-2)(n-1)}{2(nk_BT)^3}\frac{E^2}{(1+\frac{E}{nk_BT})^n}. \quad (1)$$

Here, k_B is the Boltzmann constant, E is the ion's energy, and T and n are the distribution parameters. In the limit of $n \to \infty$, the distribution becomes a 3D harmonic oscillator thermal distribution: $P(E) \propto E^2 e^{-E/k_BT}$. For finite n values, the distribution exhibits a power-law asymptotic tail: $P(E) \sim E^{2-n}$. It is also important to note that the distribution is non-normalizable for $n \leq 3$ and the distribution mean diverges for $n \leq 4$.

Our experiment [see Fig. 1(a) and Supplemental Material [34]] is designed to overlap ultracold ^{87}Rb atoms ($\sim 5\ \mu$K) trapped in a crossed dipole trap with ground-state cooled $^{88}Sr^+$ ion ($\bar{n} < 0.1$ in all three modes of motion) trapped in a linear segmented Paul trap. The ion's EMM amplitude x_{EMM}, which is the spectral part of motion oscillating at the rf frequency (Ω_{rf}), is routinely evaluated and minimized using sideband spectroscopy on a narrow optical transition. The resulting EMM energy, $E_{\mathrm{EMM}} = m_{\mathrm{ion}}(x_{\mathrm{EMM}}\Omega_{\mathrm{rf}})^2/4$, is below 0.5 mK $\cdot k_B$. Using optical pumping, we initialized the ion in the $5s^2S_{1/2}(m = -1/2)$ Zeeman sublevel [see Fig. 1(b)]. The atoms are prepared in the $F = 1$ hyperfine manifold of their electronic ground state and are not polarized [34]. We typically overlapped 20 000 atoms with the ion for a variable interaction time ranging from 0.5 ms to several seconds, at the end of which the atoms are released from the dipole trap. Following interaction, we measured the ion's energy. Different interaction times lead to different ion energies, and, therefore, two different ion-thermometry methods were used. Following short interaction times and with energies up to few mK, carrier Rabi spectroscopy [35] of the narrow electric quadrupole transition was used. For longer interaction times, we used the Doppler recooling (DRC) method [36] on a strong dipole allowed transition.

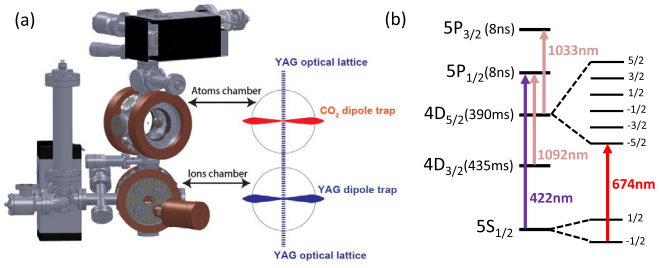

FIG. 1. (a) Experimental system. Our apparatus is composed of two vacuum chambers. In the top chamber, we collected atoms and cooled them to a temperature of several μK in a CO_2 dipole trap. We then transferred the atoms to the bottom chamber using a 1D moving optical lattice (1064 nm YAG laser) where they were retrapped in a crossed dipole trap and overlapped with a single ground-state cooled ion. (b) $^{88}Sr^+$ ion energy levels.

Each experimental run, typically lasting few seconds of atom cloud preparation, transport, and atom-ion interaction, ended with ion interrogation. Since atom-ion collisions lead to spin depolarization [30,37], we used a short optical pumping pulse to transfer the population back to the $5s^2S_{1/2}(m = -1/2)$ state before performing Rabi spectroscopy. Immediately after, we shined a pulse resonant with the $5s^2S_{1/2}(m = -1/2) \to 4d^2D_{5/2}(m = -5/2)$ narrow quadrupole transition for a duration t_R, after which we determined whether the ion was shelved to the metastable D state using state selective fluorescence on the $S_{1/2} \to P_{1/2}$ transition. The shelving probability is given by,

$$P_D(t_R) = \sum_{\mathbf{n}} P(\mathbf{n}) \sin^2(\Omega_{\mathbf{n}} t_R). \quad (2)$$

Here, $\mathbf{n} = (n_x, n_y, n_z)$ is the ion's harmonic oscillator state. $\Omega_{\mathbf{n}}$ is the carrier Rabi frequency, which depends on the ion's motional state [34]. The ion's total energy is $E = \sum_{i=x,y,z}(\hbar\omega_i n_i + 1/2)$, where $\omega_i/2\pi$ is the ith mode frequency and $\hbar$ is the reduced Planck constant. The ion's energy distribution $P(E)$ is given by Eq. (1).

The experimental results for atom-ion interaction times lasting up to 6.5 ms, which correspond to up to 20 Langevin collisions on average, are shown in Figs. 2(a)–2(f). We scanned the pulse duration t_R and fitted the measured shelving probability (shown by the filled circles) to Eq. (2) using the distribution of Eq. (1). We estimated the distribution free parameters, T and n, using maximum likelihood [34] (the best fit is shown by solid lines). As seen, the ion heats up due to collisions with the atoms, and as it does, the contrast of the flopping curve decays due to the incoherent sum of contributions from different motional states. As seen in Fig. 2(h), the energy distribution changes from thermal ($n \gg 1$) to a power-law distribution with $n = 4.0(2)$ over the course of several collisions. A comparison to the best fitted thermal distribution is shown by the dashed lines in Figs. 2(a)–2(f). As seen, a thermal distribution fails to faithfully explain our observations.

Once the energy distribution of the ion was determined, we examined the rate of ion heating as a function of the interaction time. Since the ion's mean energy is not well

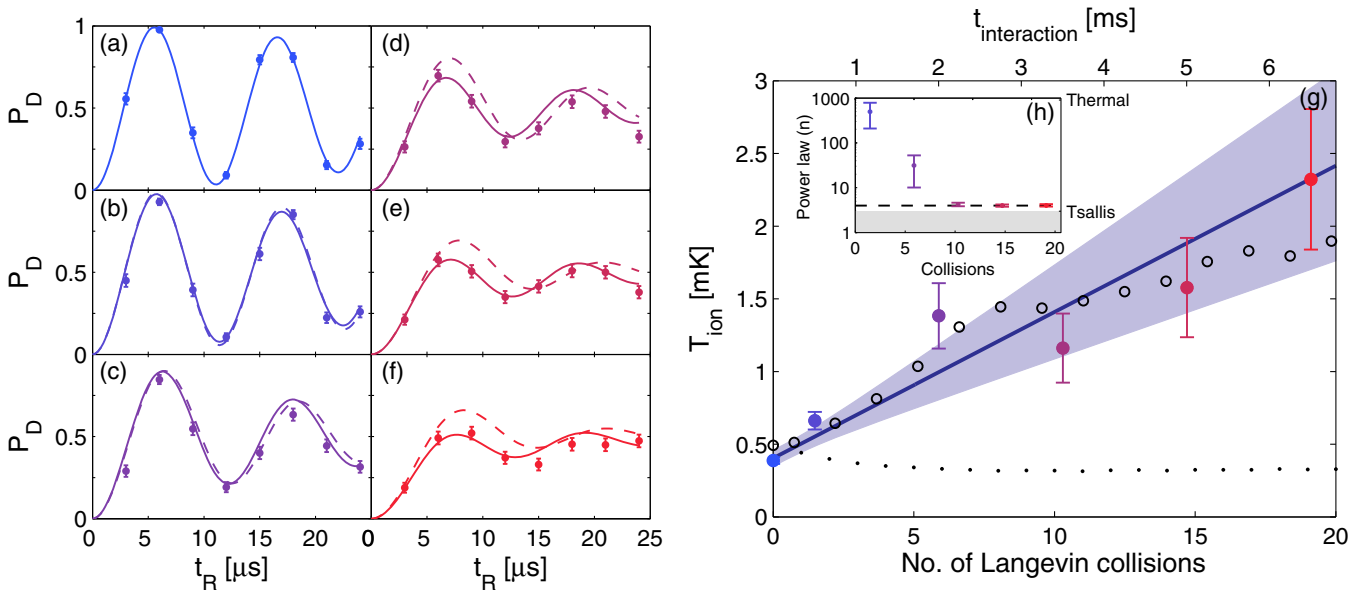

FIG. 2. Carrier Rabi spectroscopy for few atom-ion Langevin collisions. (a)–(f) Each graph corresponds to a different interaction time [0, 0.5, 2, 3.5, 5, 6.5 ms for graphs (a)–(f), respectively]. We scanned the shelving pulse time t_R and measured the shelving probability P_D. Each data point corresponds to 170 experiments. Error bars are binomial distribution standard deviation. We fitted the data using Eq. (2) together with the Tsallis distribution [Eq. (1)]. We extracted the distribution free parameters (T and n) using maximum likelihood estimation [34]. The resulting curve is shown by solid lines. Dashed lines show the fit of our data to a thermal distribution. (g) The ion's temperature [$T_{\mathrm{ion}} = Tn/(n-2)$] (filled colored circles) is plotted as function of the interaction time (top x-axis) and the average number of Langevin collisions (bottom x-axis) and it increases linearly with a rate of 296(37) μK/ms, which is equivalent to 100(13) μK per collision. Error bars are 1σ standard deviation. Shaded area represents linear fit confidence bounds (1σ). Open circles are the results of a simulation that takes into account the reaction of the polarization potential on the ion's position. Black dots are simulation results taking into account only hard-sphere collisions. (h) Ion's power-law parameter n. The ion's energy distribution starts with $n \gg 1$, consistent with a Maxwell-Boltzman distribution, and converges to $n = 4.0(2)$ after ~10 collisions. For $n > 10$, thermal and Tsallis distributions are almost indistinguishable as can be seen in (a)–(c). The gray shaded area represents the non-normalizable region of the distribution ($n < 3$). The dashed lines represent the threshold ($n = 4$) for mean energy divergence.

defined for this power law, we characterized the distribution using the most probable energy, E_{mode},

$$k_B T_{\mathrm{ion}} = E_{\mathrm{mode}}/2 = k_B Tn/(n-2), \tag{3}$$

which we will hereafter refer to as the ion's temperature. Note that for thermal distribution, $T_{\mathrm{ion}} = T$. The temperature of the ion is shown by the filled circles in Fig. 2(g). The heating is linear with a rate of 296(37) μK/ms, which corresponds to, on average, 100(13) μK per collision. After 6.5 ms, the ion's temperature exceeds 2 mK and carrier thermometry loses sensitivity. At this point, the ion has already heated up significantly beyond its EMM energy. It is important to note that even though our ion is initialized in the ground state, the first point in Fig. 2(g) is significantly higher than the ground-state temperature. This is due to beam-pointing drifts during the longer-than-a-day data acquisition time in this experiment. The beam-pointing drifts only affect the cold temperature points at which Rabi flops have high contrast [Fig. 2(a)].

To gain better understanding of the heating dynamics, we compared our results to a molecular dynamics simulation [34]. First, we used a simulation similar to Ref. [22], which only takes into account hard-sphere collisions and therefore is only affected by EMM and the atoms' temperature [black dots in Fig. 2(g)]. Here, the ion equilibrates with the residual EMM energy (set to 0.5 mK $\cdot k_B$ in the simulation). The resulting ion's energy distribution is also a power law with $n = 3.83$. However, the ion's steady-state temperature of ~0.35 mK is almost an order of magnitude lower than the last data point of our experimental results, which shows no steady-state behavior in the measured regime. As a second step, we added to our simulation the polarization force between the atom and ion and calculated the particles' trajectories in a similar fashion to Ref. [28] [empty circles in Fig. 2(g)]. In this case, the simulation faithfully reproduces our experimental results. The ion's temperature increases linearly at the experimental rate to 2 mK and the distribution power law n converges to $n = 3.8$. While the steady-state power law of the distribution is the same in both simulations, implying that the power law is independent of the heating mechanism, the resulting steady-state temperature is considerably different. As seen, in the absence of EMM and negligible atomic temperature, the ion dynamics is dominated by the reaction of the polarization potential on the ion, pulling it away from the trap center into finite rf regions

in the trap. This is the first observation of atom-ion collision dynamics that is not determined by the atom's temperature or the ion's EMM. This is also the first direct measurement of the ion's energy distribution power law. The measured power law agrees well with previous analytic [23] and simulation-based [22,33] predictions [34].

The heating rates measured using carrier Rabi spectroscopy show a linear increase in temperature throughout the entire measurement range (few mK). To measure the ion's temperature after longer interaction times, we used DRC thermometry, which is sensitive from ~10 mK to few kelvin. In DRC, the ion's fluorescence during Doppler cooling is recorded and analyzed to evaluate its initial energy [34,36]. In the recooling analysis, we took into account the eight levels involved in the DRC, cooling of all the ion modes, radiation pressure, effects of ion micromotion, and the nonthermal energy distribution of the ion [37].

To better understand the role of EMM on our ion's steady-state temperature, we scanned the EMM energy by almost 3 orders of magnitude from 0.5 to 200 mK $\cdot k_B$. We overlapped the atoms with the ion for 200 ms, during which more than 400 Langevin collisions occurred. After interaction, we detected the time-resolved fluorescence signal as it increases while the ion cools during detection. We fitted the fluorescence curve to our DRC model using the power-law distribution [Eq. (1)] with a single fit parameter T. The power-law parameter n is fixed to the value extracted from a simulation, which changes from $n = 3.9$ to 4.2 between low and high EMM energies due to the atomic cloud finite size [34]. The results are shown in Fig. 3. We observed a linear dependence of the ion's temperature with the EMM energy, $T_{\mathrm{ion}} = 0.575(19)E_{\mathrm{EMM}}/k_B + 6.8(2.4)$ mK. The scaling predicted from a simulation of hard-sphere collisions only is $T_{\mathrm{ion}} = 0.656E_{\mathrm{EMM}}/k_B$, which has a slightly higher slope, probably due to inaccuracies in DRC modeling and atomic cloud size uncertainties. However, the main difference between the simulation and the experiment is the steady-state temperature when EMM is compensated. When EMM is compensated below 0.5 mk $\cdot k_B$, a simulation of hard-sphere collisions predicts a steady-state temperature of similar magnitude [as shown in Fig. 3 by the crossing of the simulation data (black dots) at the origin], whereas our data indicate a steady-state temperature at least an order of magnitude higher. This is a second indication for dynamics beyond simple hard-sphere collisions. In the inset of Fig. 3, we show that even the DRC is sensitive, at least qualitatively, to the deviation of the ion's energy distribution from thermal (best fit shown by dashed line) to power law (similarly by solid line). Here, however, DRC is not sensitive enough to extract the exact power law from the experimental data.

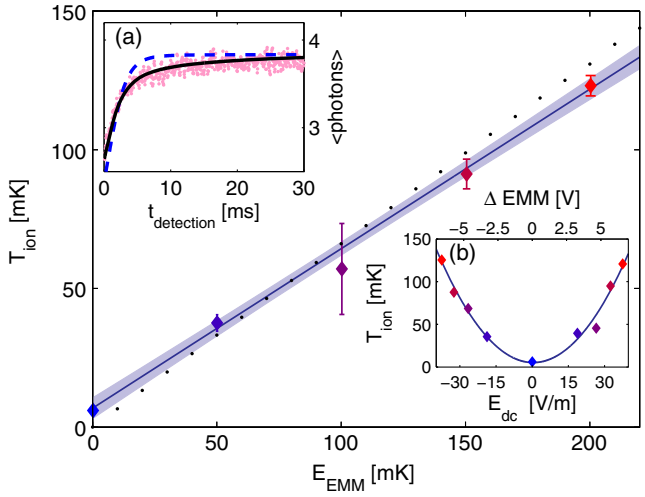

FIG. 3. Ion's steady-state temperature after hundreds of atom-ion collisions. (a) DRC signal (pink dots, 150 μs moving average) for 150 mK $\cdot k_B$ EMM experiment and a fit for power-law (black solid line) and thermal (blue dashed line) energy distributions. (b) Ion's temperature as a function of the dc electric field at the trap center (bottom x axis; top x axis shows the differential voltage on the compensation electrode). Solid blue line is a parabolic fit. In the main figure, the two opposing-sign dc voltage configurations are averaged to show the ion temperature versus the EMM kinetic energy. Error bars account for both fit confidence intervals (1σ) and the statistics of averaging over the two opposing EMM points. The solid blue line is a linear fit. Shaded area represents fit confidence bounds (1σ). The black points are the results of a simulation that takes into account only the effect of hard-sphere collisions.

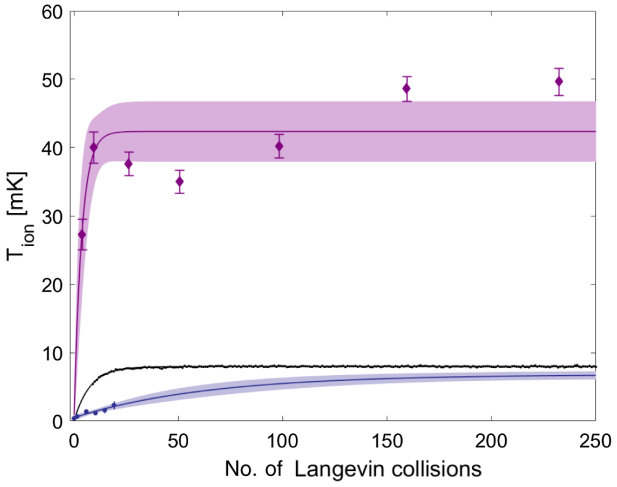

FIG. 4. Ion's heating dynamics. Ion's temperature for 100 mK $\cdot k_B$ EMM energy (purple diamonds) measured using DRC. Solid purple line is an exponential fit. Error bars are recooling fit confidence intervals (1σ). Shaded area represents fit confidence bounds (1σ). We compared this result to the heating rate measured using Rabi spectroscopy [Fig. 2(g); blue circles in this figure] and the steady-state measured using DRC (Fig. 3; not shown in this figure) for EMM energy less than 0.5 mK $\cdot k_B$. Solid blue line is an exponential fit. For comparison, we show a hard-sphere collisions simulation (black dots) with EMM energy (12 mK $\cdot k_B$), which produces the same steady-state temperature, but, however, disagrees with the heating dynamics measured.

To study the approach to steady state in the presence of EMM, we measured the ion's temperature using DRC after short interaction times. The ion's temperature in the presence of EMM with 100 mK $\cdot k_B$ average kinetic energy is plotted in Fig. 4 (magenta diamonds). From an exponential fit, we extracted a time scale $(1/e)$ of 3.6(2.8) collisions to reach steady state. We compared this collision time scale with a simulation of hard-sphere collisions, which yields a time scale $(1/e)$ of 7.7 collisions to reach steady state regardless of the EMM energy (black dots). This time scale is a signature of EMM dominated collisions where the ion quickly equilibrates with the EMM. In the absence of EMM, we observed a slow approach to steady state [64(14) collisions], which is extracted from the heating rate [100 μK per collision] measured using Rabi spectroscopy [Fig. 2(g)] and the steady state [6.8(2.4) mK] measured using DRC (Fig. 3). This observation is the third indication for different dynamics in the absence of EMM.

To conclude, our measurements characterized the deviation of the ion's energy distribution from Maxwell-Boltzmann to a power-law distribution described by the Tsallis function. This deviation from a thermal distribution was emphasized by the use of an ion-atom mixture of nearly equal-mass species. Our system can be further used to study nonequilibrium thermodynamics. We have seen that, in the regime of negligible EMM, ion heating is dominated by the pulling of the ion from the trap center by the atom. Although the steady-state temperature of our ion is far from the quantum regime, the heating rate is sufficiently slow to enable us to study ultracold interactions by preparing the ion in its electronic and motional ground state and limiting the interaction to the first few collisions.

This work was supported by the Crown Photonics Center, ICore-Israeli excellence center circle of light, the Israeli Science Foundation, the U.S.-Israel Binational Science Foundation, and the European Research Council.

[†]ziv.meir@weizmann.ac.il

[1] O. P. Makarov, R. Côté, H. Michels, and W. W. Smith, Phys. Rev. A **67**, 042705 (2003).
[2] W. W. Smith, O. P. Makarov, and J. Lin, J. Mod. Optic. **52**, 2253 (2005).
[3] A. T. Grier, M. Cetina, F. Oručević, and V. Vuletić, Phys. Rev. Lett. **102**, 223201 (2009).
[4] C. Zipkes, S. Palzer, and M. Köhl, Nature (London) **464**, 388 (2010).
[5] S. Schmid, A. Härter, and J. H. Denschlag, Phys. Rev. Lett. **105**, 133202 (2010).
[6] W. G. Rellergert, S. T. Sullivan, S. Kotochigova, A. Petrov, K. Chen, S. J. Schowalter, and E. R. Hudson, Phys. Rev. Lett. **107**, 243201 (2011).
[7] F. H. J. Hall, M. Aymar, N. Bouloufa-Maafa, O. Dulieu, and S. Willitsch, Phys. Rev. Lett. **107**, 243202 (2011).
[8] I. Sivarajah, D. S. Goodman, J. E. Wells, F. A. Narducci, and W. W. Smith, Phys. Rev. A **86**, 063419 (2012).
[9] K. Ravi, L. Seunghyun, S. Arijit, G. Werth, and S. A. Rangwala, Nat. Commun. **3**, 1126 (2012).
[10] S. Haze, S. Hata, M. Fujinaga, and T. Mukaiyama, Phys. Rev. A **87**, 052715 (2013).
[11] Z. Idziaszek, T. Calarco, P. S. Julienne, and A. Simoni, Phys. Rev. A **79**, 010702 (2009).
[12] M. Tomza, C. P. Koch, and R. Moszynski, Phys. Rev. A **91**, 042706 (2015).
[13] H. da Silva, Jr, M. Raoult, M. Aymar, and O. Dulieu, New J. Phys. **17**, 045015 (2015).
[14] R. Côté, V. Kharchenko, and M. D. Lukin, Phys. Rev. Lett. **89**, 093001 (2002).
[15] J. Joger, A. Negretti, and R. Gerritsma, Phys. Rev. A **89**, 063621 (2014).
[16] H. Doerk, Z. Idziaszek, and T. Calarco, Phys. Rev. A **81**, 012708 (2010).
[17] U. Bissbort, D. Cocks, A. Negretti, Z. Idziaszek, T. Calarco, F. Schmidt-Kaler, W. Hofstetter, and R. Gerritsma, Phys. Rev. Lett. **111**, 080501 (2013).
[18] A. Härter, A. Krükow, A. Brunner, W. Schnitzler, S. Schmid, and J. H. Denschlag, Phys. Rev. Lett. **109**, 123201 (2012).
[19] F. G. Major and H. G. Dehmelt, Phys. Rev. **170**, 91 (1968).
[20] S. J. Schowalter, A. J. Dunning, K. Chen, P. Puri, C. Schneider, and E. R. Hudson, Nat. Commun. **7**, 12448 (2016).
[21] R. G. DeVoe, Phys. Rev. Lett. **102**, 063001 (2009).
[22] C. Zipkes, L. Ratschbacher, C. Sias, and M. Köhl, New J. Phys. **13**, 053020 (2011).
[23] K. Chen, S. T. Sullivan, and E. R. Hudson, Phys. Rev. Lett. **112**, 143009 (2014).
[24] I. Rouse and S. Willitsch, Phys. Rev. A **92**, 053420 (2015).
[25] D. S. Goodman, I. Sivarajah, J. E. Wells, F. A. Narducci, and W. W. Smith, Phys. Rev. A **86**, 033408 (2012).
[26] E. Lutz, Phys. Rev. A **67**, 051402 (2003).
[27] C. Tsallis, J. Stat. Phys. **52**, 479 (1988).
[28] M. Cetina, A. T. Grier, and V. Vuletic, Phys. Rev. Lett. **109**, 253201 (2012).
[29] M. Krych and Z. Idziaszek, Phys. Rev. A **91**, 023430 (2015).
[30] L. Ratschbacher, C. Sias, L. Carcagni, J. M. Silver, C. Zipkes, and M. Köhl, Phys. Rev. Lett. **110**, 160402 (2013).
[31] L. Ratschbacher, C. Zipkes, C. Sias, and M. Köhl, Nat. Phys. **8**, 649 (2012).
[32] A. Härter, A. Krükow, A. Deisz, B. Drewa, E. Tiemann, and J. H. Denschlag, Nat. Phys. **9**, 512 (2013).
[33] B. Höltkemeier, P. Weckesser, H. López-Carrera, and M. Weidemüller, Phys. Rev. Lett. **116**, 233003 (2016).
[34] See Supplemental Material at http://link.aps.org/supplemental/10.1103/PhysRevLett.117.243401 for a detailed description of the apparatus, an explanation on the Rabi carrier spectroscopy and Doppler recooling spectroscopy methods, likelihood estimation, details on the simulations performed in this experiment, and comparison to previous analytical and simulation works.
[35] D. Leibfried, R. Blatt, C. Monroe, and D. Wineland, Rev. Mod. Phys. **75**, 281 (2003).
[36] J. H. Wesenberg, R. J. Epstein, D. Leibfried, R. B. Blakestad, J. Britton, J. P. Home, W. M. Itano, J. D. Jost, E. Knill, C. Langer, R. Ozeri, S. Seidelin, and D. J. Wineland, Phys. Rev. A **76**, 053416 (2007).
[37] T. Sikorsky, Z. Meir, R. Ben-shlomi, N. Akerman, and R. Ozeri (to be published).